

# The essence of onset and self-sustenance of turbulence in astrophysical shear flows

M. Kavtaradze <sup>\*1,2</sup>, G. Mamatsashvili<sup>†1,3</sup>, and G. Chagelishvili<sup>‡1</sup>

<sup>1</sup>Abastumani Astrophysical Observatory, Abastumani 0301, Georgia

<sup>2</sup>Department of Physics, Faculty of Exact and Natural Sciences, Javakhishvili Tbilisi State University, Tbilisi 0179, Georgia

<sup>3</sup>Helmholtz-Zentrum Dresden-Rossendorf, Bautzner Landstraße 400, D-01328 Dresden, Germany

## Abstract

To understand the mechanism of the self-sustenance of subcritical turbulence in spectrally stable astrophysical (constant) shear flows, we performed direct numerical simulations of turbulence in plane hydrodynamic and MHD homogeneous shear flows in the local shearing-box approximation with subsequent analysis of the dynamical processes in spectral/Fourier space. In the MHD case, we considered uniform magnetic field directed parallel to the flow. There are no exponentially growing modes in such flows and the turbulence is instead energetically supported only by the linear transient growth of Fourier harmonics of perturbations due to the shear flow non-normality. This non-normality-induced growth, also known as nonmodal growth, is anisotropic in Fourier space, which, in turn, leads to a specific anisotropy of nonlinear processes in this space. As a result, a main nonlinear process in shear flows is transverse (angular) redistribution of harmonics in Fourier space – nonlinear transverse cascade – rather than usual direct or inverse cascades. It is demonstrated that the turbulence is sustained by a subtle interplay between the linear nonmodal growth and the nonlinear transverse cascade for all considered flow configurations. The only energy supplier for the turbulence is the linear transient growth of perturbations due to the flow shear, which is mediated by Reynolds and Maxwell stresses, extracting, respectively, kinetic and magnetic energy from the background flow – the nonlinear processes do not directly change the total perturbation energy but only redistribute it among Fourier harmonics of perturbations. We propose the basic cycles of the turbulence sustenance in the considered cases, which clearly show the synergy of linear and nonlinear processes in the self-organization of the flow. Performing numerical simulations for different values of the background magnetic field, we show that with the increase of the field, the onset of turbulence occurs at larger times and the power of turbulence reduces. Finally, at definite threshold background magnetic field the flow completely stabilizes. It is significant that, there is an essential difference in the energy supply of plane and rotating/Keplerian astrophysical shear flows: in plane shear flows the leading linear process energetically supplying turbulence is due to the kinematics (Reynolds stress), while for Keplerian rotation – is due to magnetic field (Maxwell stress).

**Keywords:** *Astrophysical shear flows - magnetohydrodynamics - nonmodal growth - nonlinear transverse cascade - turbulence*

## 1. Introduction

Flows with shear velocity profile, where adjacent layers of matter move parallel to each other with different speeds, widely occur in nature and laboratory. For instance, they are observed in pipes, in the earth's atmosphere and – that is most important in the context of our study – are widespread in Astrophysics. So, the problem we study has a general and fundamental importance that can be applied to various astrophysical objects and observable phenomena, ranging from the intergalactic medium to the solar wind. Of course, these observable events are more complex and include kinematic and thermal effects, but the basic phenomena that occur there is a shearing motion of the matter.

Despite more than a century of history of research, until 1990s the reason of essence of turbulence onset and sustenance in spectrally stable shear flows (i.e., in flows without exponentially growing modes)

\*mariami.kavtaradze986@ens.tsu.edu.ge, Corresponding author

†g.mamatsashvili@hzdr.de

‡georgech123@yahoo.com

represented a puzzle. The turning point in understanding the physics of the shear flow turbulence was the 1990s, when the hydrodynamic instability community made a breakthrough rigorously revealing difficulties in the canonical spectral/modal approach of linear dynamics of perturbations in this type of flows. Specifically, it has been shown that the operators in the modal approach of linear processes in shear flows are exponentially far from normal (Reddy & Henningson, 1993, Schmid, 2007, Trefethen & Embree, 2005, Trefethen et al., 1993). Consequently, the eigenfunctions are not orthogonal to each other and, therefore, strongly interfere. As a result, even when all the eigenfunctions decrease monotonically in time, a particular solution may exhibit a large relative growth in a limited time interval, i.e., transient growth. This fact ultimately led to the change of canonical paradigm – the spectral/modal approach to, so-called, nonmodal approach (see e.g., Reddy et al., 1993, Trefethen et al., 1993).

As a result, a new, so-called bypass concept was developed for explaining the onset and self-sustenance of turbulence in spectrally stable shear flows (Baggett et al., 1995, Chapman, 2002, Eckhardt et al., 2007, Farrell & Ioannou, 1994, 2012, Gebhardt & Grossmann, 1994, Grossmann, 2000, Grue et al., 2014, Henningson & Reddy, 1994). It is based on the linear nonmodal growth of vortex mode perturbations due to the non-normality (shear), which is the only source of energy for turbulence in such flows. However, the transient growth itself is “imperfect” in the sense that it is not able to permanently provide energy for perturbations, so the role of nonlinear processes becomes crucial: they lie at the heart of self-sustenance of the turbulence which can be self-organized and self-sustained by a subtle interplay of the linear nonmodal and nonlinear processes.

The shear-induced transient growth mainly depends on the orientation of the perturbation wavevector: the spatial Fourier harmonics (SFHs) of perturbations having a certain orientation of the wavevector with respect to the shear flow, can draw flow energy and get amplified, whereas harmonics having other orientation of the wavevector give energy to the flow and decay. This anisotropy of linear processes in shear flows, in turn, leads to a specific anisotropy of nonlinear processes in Fourier ( $\mathbf{k}$ -) space – even in the simplest but basic HD and MHD shear flows, the dominant nonlinear process turns out to be not direct, but, so-called, transverse cascade, that is, a transverse, or angular redistribution of perturbation harmonics in  $\mathbf{k}$ -space (see e.g., Horton et al., 2010, Mamatsashvili et al., 2014).

New concepts – nonnormality, nonmodal approach, transient growth, bypass concept of subcritical turbulence – elaborated by the hydrodynamic stability community in the 1990s, was successfully adopted by atmospheric and astrophysical flow communities. The possibility of transient growth of vortex mode perturbations in hydrodynamic astrophysical/Keplerian disks was first shown by Lominadze et al. (1988). The number of studies of turbulence in astrophysical disks based on non-modal analysis has greatly increased since the 2000s (see a review Fromang & Lesur, 2019). Along this trend, in a series of recent papers Gogichaishvili et al. (2017), Gogichaishvili et al. (2018) and Mamatsashvili et al. (2020) we studied the spectral dynamics and sustenance of MHD turbulence in Keplerian flows for different magnetic field configurations. Naturally, in addition to disk flows, such an analysis is also important for plane astrophysical MHD shear flows.

In this paper, we investigate the subtle dynamic interplay of linear and nonlinear processes in subcritical MHD turbulence in shear flows. We consider three-dimensional (3D) unbounded incompressible MHD flow with a linear shear of velocity threaded by a uniform background magnetic field parallel to the flow. This flow configuration is spectrally stable in the linear regime (Ogilvie & Pringle, 1996, Stern, 1963) and therefore should be dominated by the above-mentioned shear-induced transient phenomena (Chagelishvili et al., 1997). We present the results of direct numerical simulations (DNS) in  $\mathbf{k}$ -space, demonstrating the key role of the transverse cascade in the turbulence sustenance in the considered MHD shear flow.

## 2. Physical Model and Equations

The motion of an incompressible conducting fluid is governed by the basic MHD equations:

$$\frac{\partial \mathbf{U}}{\partial t} + (\mathbf{U} \cdot \nabla) \mathbf{U} = -\frac{1}{\rho} \nabla P + \frac{(\mathbf{B} \cdot \nabla) \mathbf{B}}{4\pi\rho} + \nu \nabla^2 \mathbf{U}, \quad (1)$$

$$\frac{\partial \mathbf{B}}{\partial t} = \nabla \times (\mathbf{U} \times \mathbf{B}) + \eta \nabla^2 \mathbf{B}, \quad (2)$$

$$\nabla \cdot \mathbf{U} = 0, \quad (3)$$

$$\nabla \cdot \mathbf{B} = 0, \quad (4)$$

where  $\nu$  is the constant kinematic viscosity,  $\eta$  is Ohmic resistivity,  $\rho$  is the fluid density,  $\mathbf{U}$  is the velocity,  $\mathbf{B}$  is the magnetic field and  $P$  is the total pressure, equal to the sum of the thermal and magnetic pressures. We use the widely accepted local shearing box approximation in astrophysical disk theory where a basic flow along the  $y$  axis has a constant shear of velocity in the  $x$ -direction,  $\mathbf{U}_0 = (0, -Sx, 0)$ . This flow is threaded by a uniform magnetic field along the  $y$ -axis of the flow direction,  $\mathbf{B}_0 = (0, B_{0y}, 0)$ . Without loss of generality, the constant shear parameter and magnetic field are chosen to be positive,  $S, B_{0y} > 0$ . The equilibrium density  $\rho_0$  and total pressure  $P_0$  are spatially constant.

Consider 3D perturbations of the velocity, total pressure and magnetic field about the equilibrium flow,  $\mathbf{u} = \mathbf{U} - \mathbf{U}_0$ ,  $p = P - P_0$ ,  $\mathbf{b} = \mathbf{B} - \mathbf{B}_0$ . Substituting them into Equations (1)-(4) and rearranging the nonlinear terms with the help of divergence-free conditions (3) and (4), we arrive to the main system of Equations (20)-(27) given in Appendix, which govern the dynamics of perturbations with arbitrary amplitude. These equations are solved numerically in a 3D cubic domain with sizes  $L_x, L_y, L_z$  and resolution  $N_x \times N_y \times N_z$ , respectively, in the  $x, y$  and  $z$  directions. We use standard for the shearing box boundary conditions: shearing-periodic in  $x$  and periodic in  $y$  and  $z$ .

## 2.1. Spectral representation of the equations

Before proceeding further, we normalize the variables by taking  $S^{-1}$  as the unit of time,  $\ell$  as the arbitrary unit of length,  $S\ell$  as the unit of velocity,  $S\ell\sqrt{4\pi\rho_0}$  as the unit of magnetic field and  $\rho_0 S^2 \ell^2$  as the unit of pressure and energy. Viscosity and resistivity are measured, respectively, by Reynolds number,  $\text{Re}$ , and magnetic Reynolds number,  $\text{Rm}$ , which are defined as

$$\text{Re} = \frac{S\ell^2}{\nu}, \quad \text{Rm} = \frac{S\ell^2}{\eta}.$$

The strength of the imposed background magnetic field is measured by a parameter  $\beta = 2S^2\ell^2/u_A^2$ , where  $u_A = B_{0y}/(4\pi\rho_0)^{1/2}$  is the corresponding Alfvén speed. we decompose the perturbations into spatial Fourier harmonics (SFHs):

$$f(\mathbf{r}, t) = \int \bar{f}(\mathbf{k}, t) \exp(i\mathbf{k} \cdot \mathbf{r}) d^3\mathbf{k} \quad (5)$$

where,  $f \equiv (\mathbf{u}, p, \mathbf{b})$  denotes the perturbations and  $\bar{f} \equiv (\bar{\mathbf{u}}, \bar{p}, \bar{\mathbf{b}})$  is their corresponding Fourier transforms ( $d^3\mathbf{k} \equiv dk_x dk_y dk_z$ ).

Substituting decomposition (5) into Eqs.(20)-(27) and taking into account the above normalization, we arrive at the following equations governing the dynamics of perturbation SFHs in Fourier space:

$$\frac{\partial}{\partial t} \frac{|\bar{u}_x|^2}{2} = -k_y \frac{\partial}{\partial k_x} \frac{|\bar{u}_x|^2}{2} + \mathcal{H}_x + \mathcal{I}_x^{(ub)} + \mathcal{D}_x^{(u)} + \mathcal{N}_x^{(u)}, \quad (6)$$

$$\frac{\partial}{\partial t} \frac{|\bar{u}_y|^2}{2} = -k_y \frac{\partial}{\partial k_x} \frac{|\bar{u}_y|^2}{2} + \mathcal{H}_y + \mathcal{I}_y^{(ub)} + \mathcal{D}_y^{(u)} + \mathcal{N}_y^{(u)}, \quad (7)$$

$$\frac{\partial}{\partial t} \frac{|\bar{u}_z|^2}{2} = -k_y \frac{\partial}{\partial k_x} \frac{|\bar{u}_z|^2}{2} + \mathcal{H}_z + \mathcal{I}_z^{(ub)} + \mathcal{D}_z^{(u)} + \mathcal{N}_z^{(u)}, \quad (8)$$

$$\frac{\partial}{\partial t} \frac{|\bar{b}_x|^2}{2} = -k_y \frac{\partial}{\partial k_x} \frac{|\bar{b}_x|^2}{2} + \mathcal{I}_x^{(bu)} + \mathcal{D}_x^{(b)} + \mathcal{N}_x^{(b)} \quad (9)$$

$$\frac{\partial}{\partial t} \frac{|\bar{b}_y|^2}{2} = -k_y \frac{\partial}{\partial k_x} \frac{|\bar{b}_y|^2}{2} + \mathcal{M} + \mathcal{I}_y^{(bu)} + \mathcal{D}_y^{(b)} + \mathcal{N}_y^{(b)} \quad (10)$$

$$\frac{\partial}{\partial t} \frac{|\bar{b}_z|^2}{2} = -k_y \frac{\partial}{\partial k_x} \frac{|\bar{b}_z|^2}{2} + \mathcal{I}_z^{(bu)} + \mathcal{D}_z^{(b)} + \mathcal{N}_z^{(b)}, \quad (11)$$

which are the main equations for the subsequent analysis. They serve as the mathematical basis for understanding of the interplay of the dynamical processes sustaining the subcritical turbulence in the considered shear flow. The right-hand side (rhs) terms of the above dynamical equations describe processes of linear,  $\mathcal{H}_i(\mathbf{k}, t)$ ,  $\mathcal{I}_i^{(ub)}(\mathbf{k}, t)$ ,  $\mathcal{I}_i^{(bu)}(\mathbf{k}, t)$ ,  $\mathcal{M}(\mathbf{k}, t)$ , and nonlinear,  $\mathcal{N}_i^{(u)}(\mathbf{k}, t)$ ,  $\mathcal{N}_i^{(b)}(\mathbf{k}, t)$ , origin, where the index

$i = x, y, z$  henceforth.  $\mathcal{D}_i^{(u)}(\mathbf{k}, t)$  and  $\mathcal{D}_i^{(b)}(\mathbf{k}, t)$  terms, describing viscous and resistive dissipation, are negative definite. The linear terms are:

$$\mathcal{H}_x = -2\frac{k_x k_y}{k^2} |\bar{u}_x|^2, \quad \mathcal{H}_y = \left( \frac{1}{2} - \frac{k_y^2}{k^2} \right) (\bar{u}_x \bar{u}_y^* + \bar{u}_x^* \bar{u}_y), \quad \mathcal{H}_z = -\frac{k_y k_z}{k^2} (\bar{u}_x \bar{u}_z^* + \bar{u}_x^* \bar{u}_z),$$

$$\mathcal{M} = -\frac{1}{2}(\bar{b}_x \bar{b}_y^* + \bar{b}_x^* \bar{b}_y), \quad \mathcal{I}_i^{(ub)} = \frac{i}{2} k_y B_{0y} (\bar{u}_i^* \bar{b}_i - \bar{u}_i \bar{b}_i^*), \quad \mathcal{I}_i^{(bu)} = -\mathcal{I}_i^{(ub)}$$

$$\mathcal{D}_i^{(u)} = -\frac{k^2}{\text{Re}} |\bar{u}_i|^2, \quad \mathcal{D}_i^{(b)} = -\frac{k^2}{\text{Rm}} |\bar{b}_i|^2.$$

Here  $\mathcal{H}_x, \mathcal{H}_y, \mathcal{H}_z$  are the energy injection terms for the corresponding velocity components, while their sum  $\mathcal{H} = \mathcal{H}_x + \mathcal{H}_y + \mathcal{H}_z = (\bar{u}_x \bar{u}_y^* + \bar{u}_x^* \bar{u}_y)/2$  is Reynolds stress spectrum,  $\mathcal{M}$  is the Maxwell stress spectrum,  $\mathcal{I}_i^{(ub)}(\mathbf{k}, t), \mathcal{I}_i^{(bu)}(\mathbf{k}, t)$  are terms that describe the linear exchange between kinetic and magnetic energies and  $k^2 = k_x^2 + k_y^2 + k_z^2$ . The modified nonlinear transfer functions  $\mathcal{N}_i^{(u)}(\mathbf{k}, t)$  for the quadratic forms of the velocity components are:

$$\mathcal{N}_i^{(u)} = \frac{1}{2} (\bar{u}_i Q_i^* + \bar{u}_i^* Q_i). \quad (12)$$

where

$$Q_i = i \sum_j k_j N_{ij}^{(u)} - i k_i \sum_{m,n} \frac{k_m k_n}{k^2} N_{mn}^{(u)}, \quad i, j, m, n = x, y, z. \quad (13)$$

and

$$N_{ij}^{(u)}(\mathbf{k}, t) = \int d^3 \mathbf{k}' [\bar{b}_i(\mathbf{k}', t) \bar{b}_j(\mathbf{k} - \mathbf{k}', t) - \bar{u}_i(\mathbf{k}', t) \bar{u}_j(\mathbf{k} - \mathbf{k}', t)] \quad (14)$$

The nonlinear terms for the quadratic forms of the magnetic field components are

$$\mathcal{N}_x^{(b)} = \frac{i}{2} \bar{b}_x^* [k_y \bar{F}_z - k_z \bar{F}_y] + c.c.,$$

$$\mathcal{N}_y^{(b)} = \frac{i}{2} \bar{b}_y^* [k_z \bar{F}_x - k_x \bar{F}_z] + c.c., \quad (15)$$

$$\mathcal{N}_z^{(b)} = \frac{i}{2} \bar{b}_z^* [k_x \bar{F}_y - k_y \bar{F}_x] + c.c.$$

where  $i, j = x, y, z$  and  $\bar{F}_x, \bar{F}_y, \bar{F}_z$  are the Fourier transforms of the respective components of the perturbed electromotive force:  $\mathbf{F} = \mathbf{u} \times \mathbf{b}$ ,

$$\bar{F}_x(\mathbf{k}, t) = \int d^3 \mathbf{k}' [\bar{u}_y(\mathbf{k}', t) \bar{b}_z(\mathbf{k} - \mathbf{k}', t) - \bar{u}_z(\mathbf{k}', t) \bar{b}_y(\mathbf{k} - \mathbf{k}', t)], \quad (16)$$

$$\bar{F}_y(\mathbf{k}, t) = \int d^3 \mathbf{k}' [\bar{u}_z(\mathbf{k}', t) \bar{b}_x(\mathbf{k} - \mathbf{k}', t) - \bar{u}_x(\mathbf{k}', t) \bar{b}_z(\mathbf{k} - \mathbf{k}', t)], \quad (17)$$

$$\bar{F}_z(\mathbf{k}, t) = \int d^3 \mathbf{k}' [\bar{u}_x(\mathbf{k}', t) \bar{b}_y(\mathbf{k} - \mathbf{k}', t) - \bar{u}_y(\mathbf{k}', t) \bar{b}_x(\mathbf{k} - \mathbf{k}', t)], \quad (18)$$

One can distinguish five basic processes in Equations (6)-(11), that underlie the dynamics of perturbations:

- 1) The first terms on the rhs are of linear origin and describe advection, or "drift" of perturbation harmonics in Fourier space with the normalized velocity  $k_y$ . They travel along the  $k_x$  - axis for harmonics with  $k_y > 0$  and opposite for  $k_y < 0$  ones, the ones with  $k_y = 0$  are not advected by the flow.
- 2) The second terms of the rhs of Equations (6)-(8) and (10), are associate with the shear, they originate from the linear terms proportional to the shear parameter and are therefore also of linear origin. They describe energy exchange between the mean flow and individual SFHs. These terms are responsible for providing energy for perturbations so that they can amplify. In the present case, such amplification is due to the shear flow non-normality.  $\mathcal{H}$  and  $\mathcal{M}$  are related to the volume - averaged nondimensional Reynolds and Maxwell stresses. As was mentioned above since perturbation harmonics undergo the drift in  $\mathbf{k}$ -space, their amplification has a transient nature (Chagelishvili et al., 2003, Farrell & Ioannou, 1993, Gustavsson, 1991, Tevzadze et al., 2003). So, these linear terms are a main source of energy for SFHs.

- 3) The cross terms,  $\mathcal{I}_i^{(ub)}$  and  $\mathcal{I}_i^{(bu)}$  are also of linear origin and describe the exchange between kinetic and magnetic spectral energies. They have opposite signs and therefore cancel out in the total energy budget of SFHs. So, they do not generate new energy for harmonics, but rather exchange between kinetic and magnetic components.
- 4) The terms  $\mathcal{D}_i^{(u)}$  and  $\mathcal{D}_i^{(b)}$  are of linear origin and negative definite, they describe, respectively, the dissipation of kinetic and magnetic energies due to viscosity and resistivity. Comparing these dissipation terms with the energy-supplying terms  $\mathcal{H}_i$  and  $\mathcal{M}$ , it is evident that dissipation is important at large wavenumbers  $k \gtrsim k_D \equiv \min(\sqrt{\text{Re}}, \sqrt{\text{Rm}})$ .
- 5) The nonlinear terms  $\mathcal{N}_i^{(u)}$  and  $\mathcal{N}_i^{(b)}$  (Equations (12) and (15)) describe nonlinear redistribution, or transfer, respectively, of kinetic and magnetic energies among SFHs with different wavenumbers in Fourier space. From the definition of these terms their sum integrated over an entire wavenumber space is zero,

$$\int [\mathcal{N}^{(u)}(\mathbf{k}, t) + \mathcal{N}^{(b)}(\mathbf{k}, t)] d^3\mathbf{k} = 0, \quad (19)$$

This implies that the main effect of nonlinearity is only to redistribute (scatter) the energy of perturbation harmonics, that was drawn from the background flow by the Reynolds and Maxwell stresses, over wavenumbers and among each other, while leaving the total spectral energy summed over all wavenumbers unchanged. These nonlinear transfer functions,  $\mathcal{N}_i^{(u)}$  and  $\mathcal{N}_i^{(b)}$  play a central role in subcritical MHD turbulence theory – they determine cascades of energies in  $\mathbf{k}$ -space, leading to the development of their specific spectra (Alexakis et al., 2007, Verma, 2004). These transfer functions are one of the main focuses of the present analysis. Our purpose is to explore how these functions operate in the presence of the flow shear and the background magnetic field parallel to the flow. In particular, we will demonstrate below that, similar to the cases studied in 2D HD and MHD plane, as well as in previously studied Keplerian shear flows (Gogichaishvili et al., 2017, 2018, Horton et al., 2010, Mamatsashvili et al., 2014, 2020) the energy spectra, energy injection, and nonlinear transfers are also anisotropic in the quasi-steady subcritical turbulence, resulting in the redistribution of spectral energy among wavevector angles in  $\mathbf{k}$ -space, which is referred to as the nonlinear transverse cascade, in contrast to the canonical direct cascade.

### 3. Simulations and General Characteristics

We solve Equations (20)-(27) of the Appendix using the pseudospectral code SNOOPY Lesur & Longaretti (2007), which is a general purpose code, solving HD and MHD equations, including shear, rotation, stratification, and several other physical effects. Fourier transforms are computed using the FFTW library. Nonlinear terms are computed using a pseudo-spectral algorithm and antialiasing is enforced using the 2/3 rule. Time integration is done by a standard explicit third-order Runge–Kutta scheme and for viscous and resistive terms is used an implicit scheme. The code has been tested and extensively used in a number of fluid dynamical and astrophysical contexts. The initial conditions consist of small amplitude random noise perturbations of the velocity and magnetic field with spatially uniform rms amplitudes  $\langle \mathbf{u}^2 \rangle^{1/2} = \langle \mathbf{b}^2 \rangle^{1/2} = 0.6$  on top of the shear flow. The computational domain has sizes  $(L_x, L_y, L_z) = (2\pi, 2\pi, 2\pi)$  and numerical resolution  $(N_x, N_y, N_z) = (256, 256, 256)$ . The viscous and resistive Reynolds numbers are fixed to the values  $R_e = R_m = 1000$ . The subsequent time-evolution with these initial conditions was followed to  $t_f = 1000$  (i.e., for a total of 1000 shear times).

Figure 1 shows the time-development of the volume-averaged perturbed kinetic,  $E_K$ , and magnetic,  $E_M$ , energy densities for different initial magnetic field strengths,  $B_{0y} = 0; 0.1, 0.3; 0.35$ . At the early stage of evolution, the initially imposed small perturbations start to grow as a result of transient amplification, due to the flow non-normality of separate SFHs contained in the initial conditions. Then, after several orbits the perturbation amplitude becomes high enough for the nonlinearity to be triggered. After reaching the nonlinear regime, the flow eventually settles down into a sustained quasi-steady subcritical MHD turbulence that persists until the end of the simulation. It is clearly seen in Figure 1, that the kinetic energy dominates the magnetic one and as the value of the initial magnetic field increases, the kinetic as well as magnetic energy decrease in magnitude, and after reaching a critical value  $B_{0y,c} \approx 0.33$  the turbulence disappears.

Figure 2 shows the time development of the volume-averaged Reynolds,  $\langle u_x u_y \rangle$ , and Maxwell,  $\langle -b_x b_y \rangle$ , stresses for different initial magnetic field strengths,  $B_{0y} = 0; 0.1, 0.3; 0.35$ . In all the cases, the Reynolds

stress is larger than the Maxwell stress. This indicates that the energy extraction from the mean flow are dominated by the velocity perturbations in 3D MHD shear flows rather than by magnetic field ones, which actually take energy from the velocity perturbations. Similarly, we see that the increase of the background magnetic field  $B_{0y}$  leads to the decay of the turbulence. So, the Reynolds stress plays a vital role in counteracting dissipation and ensuring turbulence sustenance by continuously replenishing transiently growing modes that themselves alone would be incapable of long-term supply of turbulence.

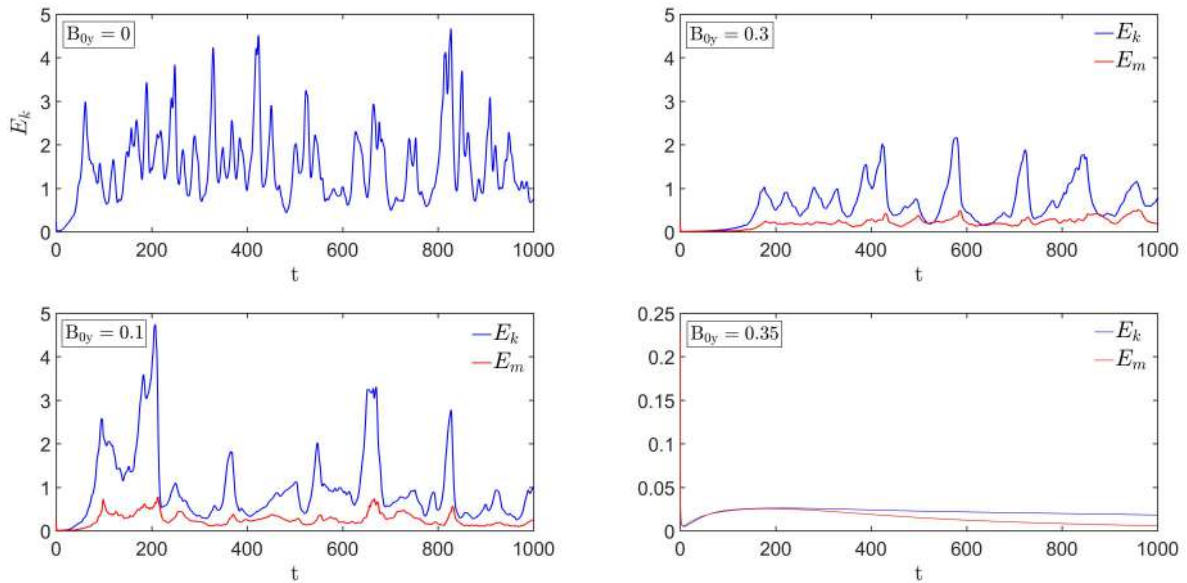


Figure 1. Evolution of the volume-averaged kinetic (blue) and magnetic (red) energy densities for different initial magnetic field strengths  $B_{0y} = 0; 0.1, 0.3; 0.35$ . Turbulence sets in after several orbits, with the kinetic energy dominating magnetic one. As the value of the mean magnetic field increases, turbulence decays.

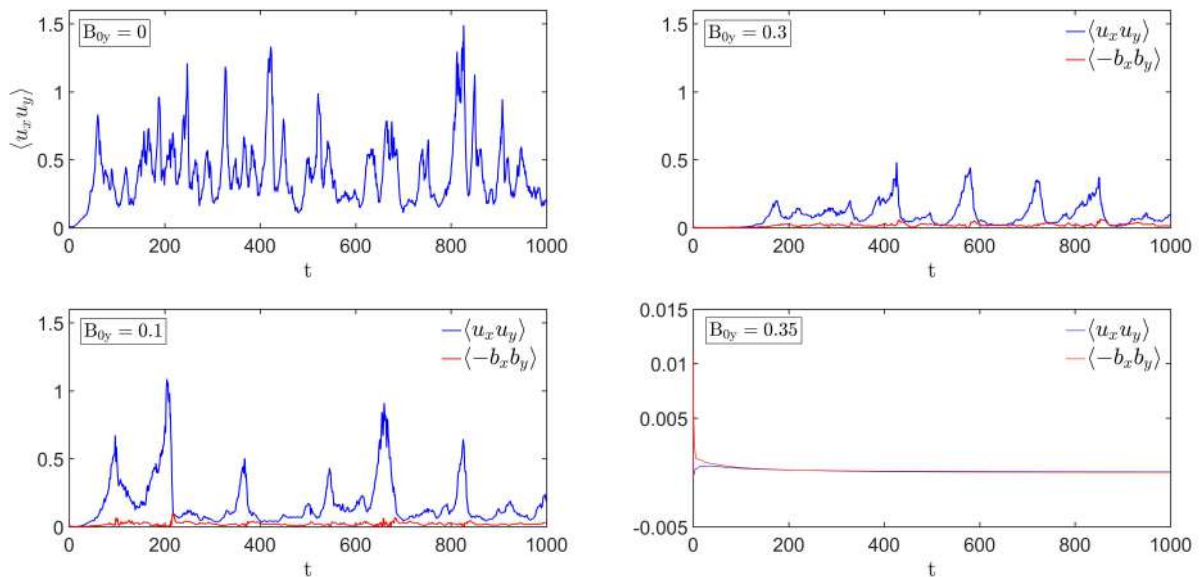


Figure 2. Evolution of the volume-averaged Reynolds (blue) and Maxwell (red) stresses for different initial magnetic field strengths  $B_{0y} = 0; 0.1, 0.3; 0.35$ . In all cases, Reynolds stress dominates over Maxwell stress.

In contrast to the present case with no rotation, in the 3D MHD Keplerian flow, which represents combination of rotation and shear, with an azimuthal mean magnetic field, energy extraction from the background flow is mostly due to Maxwell stress, as shown in Figure 3 (reproduced from Gogichaishvili et al., 2017). It is interesting to note that the dominance of Maxwell stress is observed in all other cases of 3D MHD turbulence with Keplerian flows and different magnetic field configurations (Gogichaishvili et al., 2018, Mamatsashvili et al., 2020). The Maxwell stress is also much larger than the Reynolds stress in the

2D MHD case (Mamatsashvili et al., 2014), signifying that the energy extraction from the mean flow is dominated by the magnetic field perturbations. Moreover, this study has shown that the Reynolds stress not only has a smaller magnitude than the Maxwell stress but also has a negative sign, thereby indicating that it does not contribute to the gain in turbulent kinetic energy.

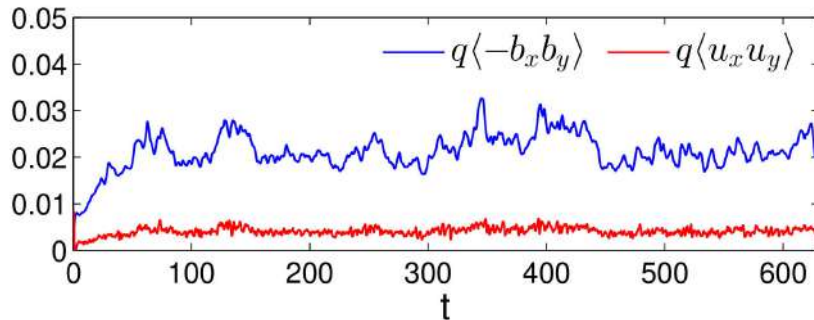


Figure 3. Evolution of the volume-averaged Reynolds (red) and Maxwell (blue) stresses for Keplerian disk with an azimuthal magnetic field (Gogichaishvili et al., 2017). Here Maxwell stress dominates Reynolds stress contrary to the 3D MHD plane case.

### 3.1. Analysis in Fourier Space

Deeper insight into the nature of the dynamics of the 3D MHD subcritical turbulence can be gained by performing analysis in Fourier space. In general, as demonstrated in previous works (Gogichaishvili et al., 2017, Mamatsashvili et al., 2014) to understand the dynamics of the quasi-steady turbulence state, each linear and nonlinear term of the spectral equations (6)-(11) should be calculated explicitly and visualized in Fourier space. But without a loss of generality in this proceedings paper, we will only focus on the  $x$ -component of the velocity field (Equation 6), as it was seen from the previous section, the kinetic processes prevail over magnetic ones, and since the shear is along the  $x$ -direction, the basic cycle can be closed for the  $x$ -component. To visualize each component of Equation (6) in Fourier space we use simulation data from The Snoopy Code and focus on the case  $B_{0y} = 0.1$ . Before proceeding to spectral analysis, it should be mentioned that all of the spectral quantities/terms in the above equation are averaged in time over an entire saturated/quasi-steady turbulent state, between  $t = 100$  and the end of the run at  $t_f = 1000$ .

Certainly, three-dimensionality complicates the analysis. Therefore, we first find out which vertical wavenumbers are important. Hence, we integrate the spectral energies and stresses in the  $(k_x, k_y)$ -plane and represent as a function of  $k_z$  (figure 4). It is evident that the kinetic and magnetic energies, along with the Reynolds and Maxwell stresses, reach their maximum values at small  $k_z$  and rapidly decrease as  $k_z$  increases, implying that the turbulence-maintaining processes predominantly occur at small wavenumbers. This energy-containing area in  $\mathbf{k}$ -space is called the *vital area*. So, below we will focus on the dynamics at small  $k_z$  and, specifically, show the dynamical terms at  $k_z = 0, 1, 2$ .

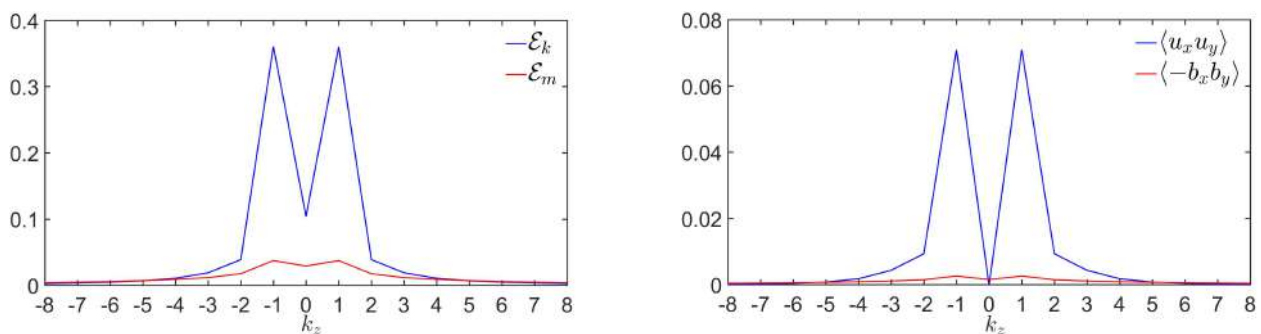


Figure 4. Time-averaged kinetic,  $\mathcal{E}_k$ , and magnetic,  $\mathcal{E}_m$ , energy spectra (left panel), also Reynolds,  $\langle u_x u_y \rangle$ , and Maxwell,  $\langle -b_x b_y \rangle$ , stresses (right panel) integrated in  $(k_x, k_y)$  plane and represented as a function of  $k_z$ .

drift term along  $k_x$ , injection term,  $\mathcal{H}_x$ , and the nonlinear transfer term,  $\mathcal{N}_x^{(u)}$ , in  $(k_x, k_y)$ -plane at  $k_z = 0, 1, 2$  (figure 5). It is clear from these plots that the  $|\bar{u}_x|$  spectrum, as well as the linear and nonlinear terms are anisotropic, i.e., strongly depend on the wavevector angle. This specific anisotropy is due to the flow shear.

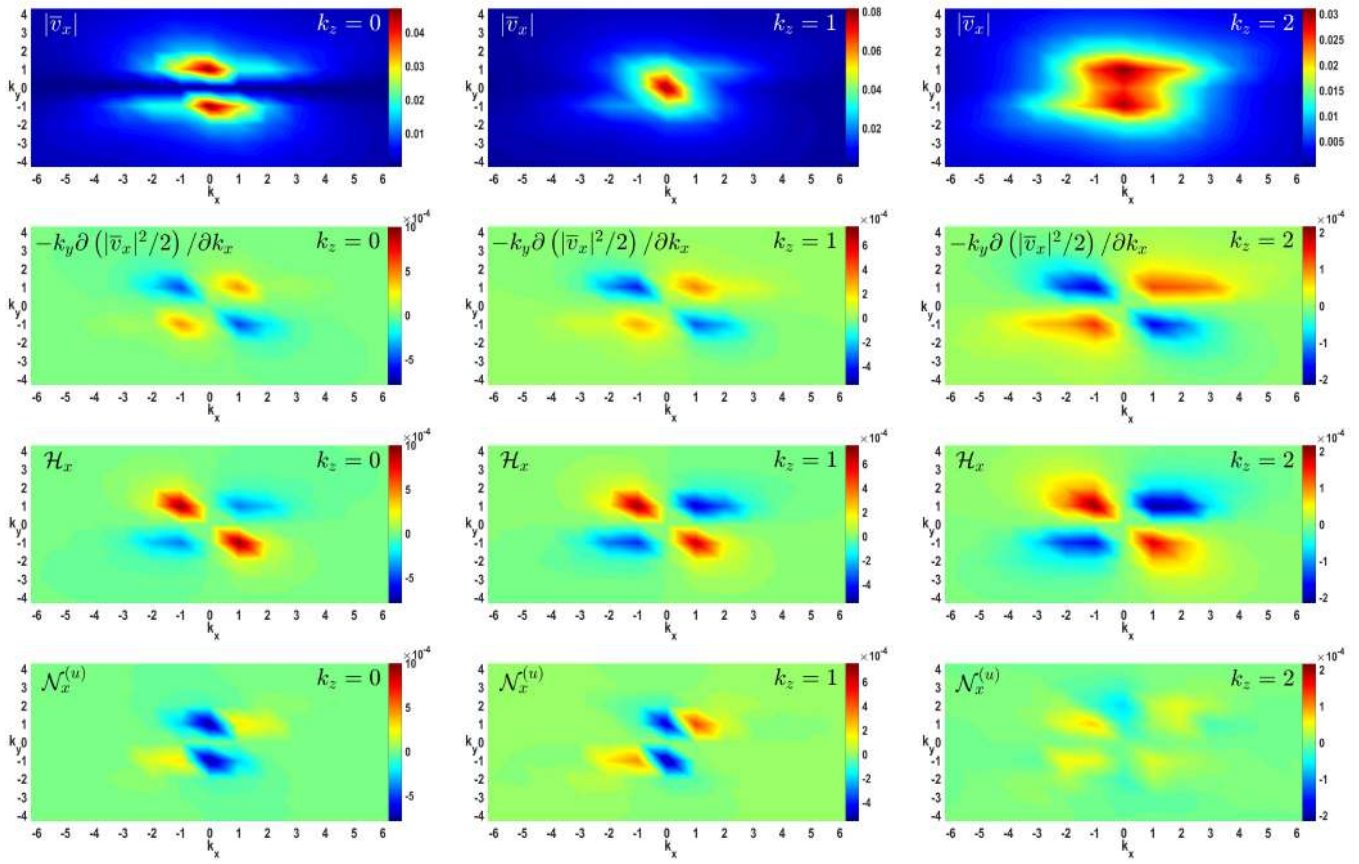


Figure 5. Spectra of  $|\bar{u}_x|$  (upper row) together with the linear drift (second row), injection  $\mathcal{H}_x$  (third row) and nonlinear  $\mathcal{N}_x^{(u)}$  (fourth row) terms in the  $(k_x, k_y)$ -plane at  $k_z = 0$  (left), 1 (middle) and 2 (right) slices. These terms mainly operate at small wavenumbers  $k \lesssim 3$ . In the red and yellow regions dynamical terms are positive, in the blue and dark blue regions they are negative and in the light green regions they are small.

The dynamics of  $|\bar{u}_x|$  is primarily determined by the combined action of the drift  $(-k_y \partial(|\bar{u}_x|^2/2)/\partial k_x)$ , injection ( $\mathcal{H}_x$ ), and the nonlinear ( $\mathcal{N}_x^{(u)}$ ) terms. Here we do not show viscous term,  $\mathcal{D}_i^{(u)}$ , because its action is simple – it is always negative and reduces the corresponding quantities. Namely, it increases with  $k$ , but in the vital area is too small and does not influence the dynamics. The linear cross terms,  $\mathcal{I}_x^{(ub)}$  and  $\mathcal{I}_x^{(bu)}$ , as was mentioned above, describe the exchange between kinetic and magnetic spectral energies. These terms are also small compared to other dynamical terms and do not play any notable role in the sustenance of turbulence (and hence is not shown in Figure 5).

The second row of Figure 5 shows the linear drift of SFHs. This process transfers perturbation modes with normalized velocity  $k_y$ , along the  $k_x$ -axis for  $k_y > 0$  and in the opposite direction for  $k_y < 0$ , due to shear. Namely, harmonics drift from blue and dark blue regions (energy decrease) to red and yellow regions (energy increase). It should be mentioned that streamwise constant harmonics, with  $k_y = 0$ , are not affected by the drift.

The third row of Figure 5 shows the action of the injection term  $\mathcal{H}_x$ . As was demonstrated in the previous section, Reynolds stress is positive and larger than Maxwell stress, so it is mainly responsible for the energy supply of the turbulence, as it exchanges energy between the background shear flow and perturbations. Where the  $x$ -component of the injection term is positive (red and yellow regions in the third row of Figure 5), it increases the energy of the  $x$  component of perturbed velocity, and in the regions where it is negative (blue and dark blue regions), it takes kinetic energy from this velocity component and gives it back to the flow. Thus Reynolds stress is the main energy supplier for the turbulence. It ensures energy injection into the turbulent fluctuations.

The fourth row of Figure 5 demonstrates the action of the nonlinear transfer  $\mathcal{N}_x^{(u)}$ . This function redistributes the energy of the  $x$ -component of velocity  $|\bar{u}_x|^2/2$  not only along the wave vector, as in the

direct cascade, but also transversely to the wavevector from the blue and dark blue regions, where  $\mathcal{N}_x^{(u)} < 0$ , to the red and yellow regions, where  $\mathcal{N}_x^{(u)} > 0$ . It is apparent from Figure 5 that the dependence of this term on the polar angle is influenced by the shear, leading to a redistribution of spectral energy across wavevector angles. This relatively new process known as the nonlinear transverse cascade fundamentally differs from the canonical direct cascade, where energy is directly transferred from small wavevectors (large scales) to large ones (small scales), where it is dissipated. As we will see below, the transverse cascade is essential for the self-sustenance of the considered subcritical turbulence.

### 3.2. Interplay of the Linear and Nonlinear Processes

Now that we have outlined the dynamical balances in Fourier space, we can proceed to construct, based on them, the main self-sustaining scheme/cycle of 3D MHD subcritical turbulence. As was mentioned above, due to the substantial difference in magnitude and importance between the kinetic energy and Reynolds stress compared to the magnetic energy and Maxwell stress, it can be concluded that the sustenance is predominantly driven by kinematics of the flow.

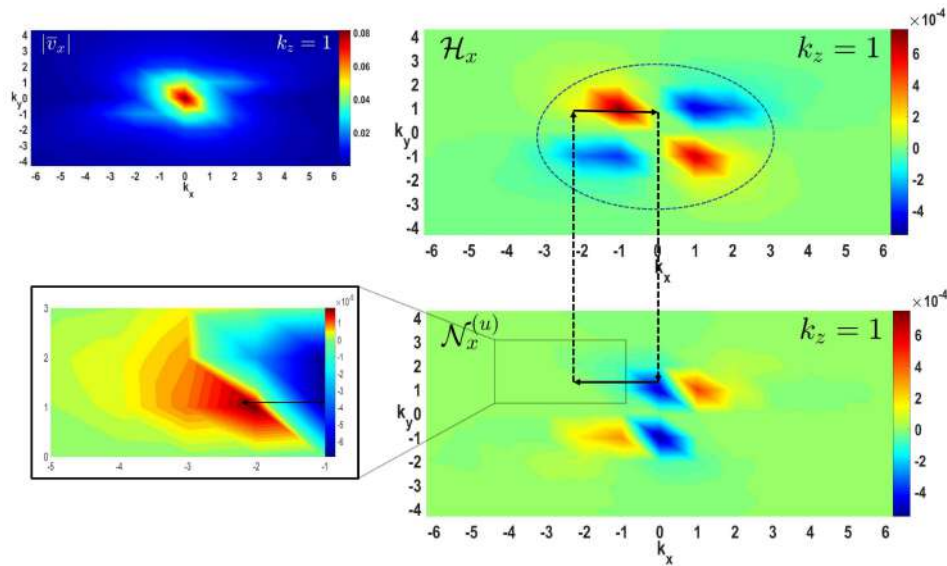


Figure 6. Scheme of the basic cycle of turbulence sustenance. In the circle, there is the vital area. The solid arrow in the plot of  $\mathcal{H}_x$  represents the linear drift of perturbations from left to right. The right dashed arrow redirects the same wavevector to the  $\mathcal{N}_x^{(u)}$  plot to show the processes occurring there. The solid arrow in the plot of  $\mathcal{N}_x^{(u)}$  represents the nonlinear transfer (transverse cascade) of kinetic energy from right to left. The left dashed arrow redirects the same wavevector to the  $\mathcal{H}_x$  plot, where, once again due to the drift, perturbations have the opportunity to pass the energy injection area and amplify and then, via  $\mathcal{N}_x^{(u)}$  regenerate new modes reentering the amplification area again, thereby closing the sustenance cycle. These processes contribute to the spectra of  $|\bar{u}_x|$  (shown in the top left plot).

The central aspect of this process should revolve around the dominant  $k_z$  slice ( $k_z = 1$ ) of the  $x$ -component of the velocity field, which carries the most energy, particularly at wavenumbers where its magnitude is significant, specifically within the vital area. So, now we can construct the basic cycle of self-sustenance of turbulence based on the information presented in Figure 6. The basic cycle is as follows – harmonics located in the amplification quadrant II, in the plot of  $\mathcal{H}_x$ , drift along the  $k_x$ -axis from left to right due to shear, as represented by the solid arrow. The nonlinear function  $\mathcal{N}_x^{(u)}$  transfers part of the kinetic energy from the amplified harmonics from right to left, represented by the solid arrow, to the amplification area, where  $\mathcal{H}_x > 0$ . This process regenerates harmonics having the potential of growth within the vital area, ultimately closing the cycle and realizing a positive nonlinear feedback, thereby sustaining the turbulence. So, the realization of positive feedback would not be possible without the existence of the transverse cascade,

which, in this case, dominates over the nonlinear direct cascade. It transfers perturbation harmonics to the amplification part of the vital area, contrasting with the direct cascade, which takes away harmonics from the vital area and transfers them to small/dissipative scales. It is important to note that when studying anisotropic turbulence, using only the direct cascade is misleading. The presence of anisotropy introduces the existence of the transverse cascade and competition between these two nonlinear processes becomes crucial in determining whether turbulence will be sustained or not. Namely, if the transverse cascade prevails over the direct one, the turbulence will be sustained. Conversely, if the direct cascade prevails over the transverse one, the turbulence will decay.

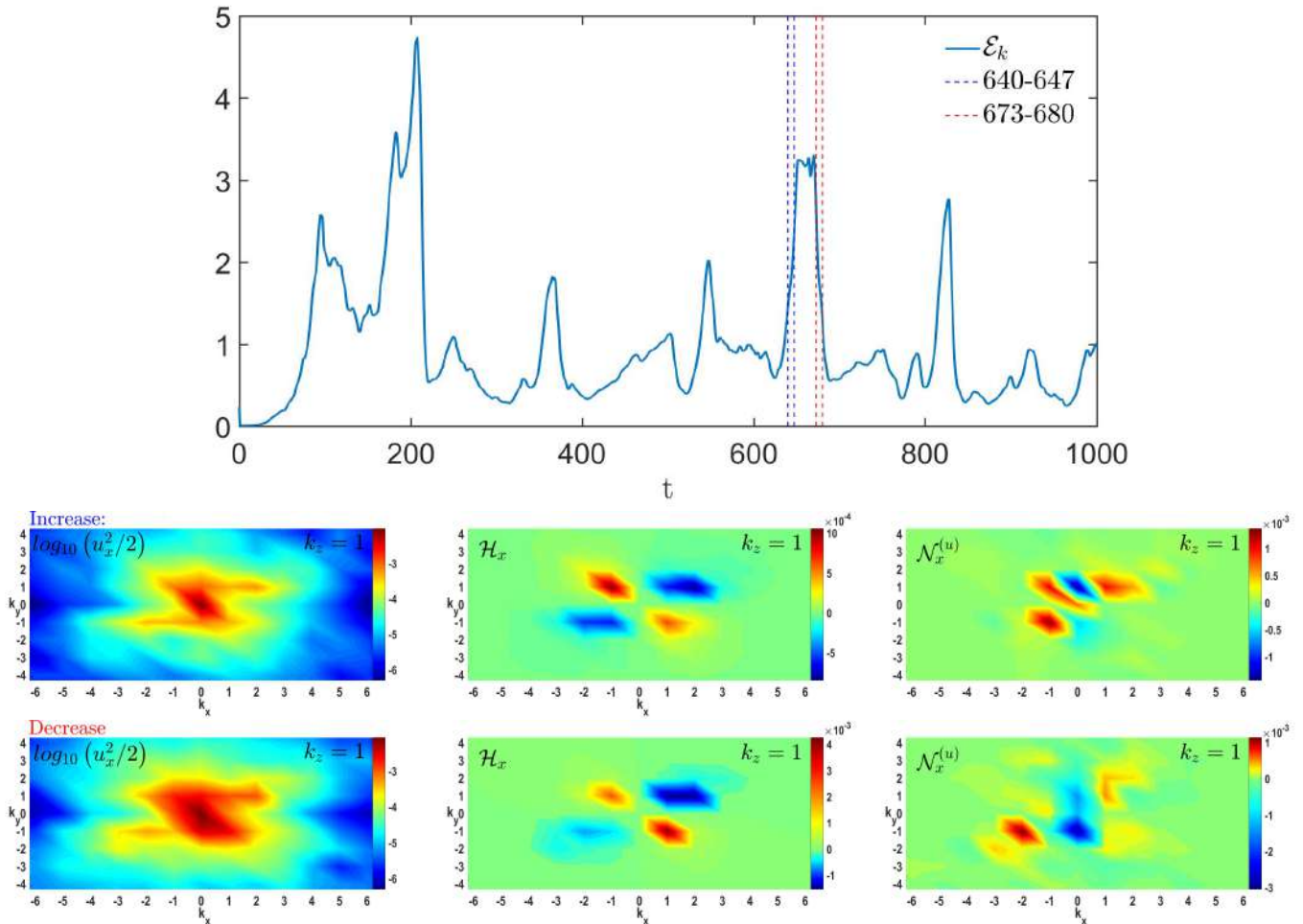


Figure 7. The upper plot shows the evolution of the volume-averaged kinetic energy, where the intervals of increase,  $t = 640 - 647$ , and decrease,  $t = 673 - 680$ , around the peak during which the spectral quantities are analyzed below are denoted with vertical dashed lines. The spectra of  $|\bar{u}_x|^2/2$  (left column), injection term  $\mathcal{H}_x$  (middle column) and nonlinear transfer term  $\mathcal{N}_x^{(u)}$  (right column) are shown during the increase (middle row) and decrease (bottom row) phases of kinetic energy. From the right plot of the transfer term during the increase stage it is seen that mode with wavevector  $\mathbf{k} = (0, 0, 1)$  gains energy ( $\mathcal{N}_x^{(u)}(0, 0, 1) > 0$ ) whereas, during the decrease regime, energy is transferred away from this mode ( $\mathcal{N}_x^{(u)}(0, 0, 1) < 0$ ).

So far, we have averaged the spectral quantities in time over an entire saturated turbulent state and study their dynamics and role in the sustenance of turbulence. However, it is also interesting to observe the processes that occur within small time intervals, which we have done. As we see in the first plot of the Figure 7, the turbulent field has a quite noisy nature – the energy curve has peaks/bursts in the quasi-steady state. By averaging spectral quantities/terms over the entire saturated turbulent state, we can gain an understanding of the general behavior of these terms. Still, during this procedure, a lot of essential information is lost. Therefore, we performed averaging of physical quantities within a small time interval, specifically, during the increase ( $t = 640 - 647$ ) and during the decrease ( $t = 673 - 680$ ) stages of the kinetic energy, as depicted in the upper plot of Figure 7. During the increasing regime, nonlinearity transfers energy to the wavevector, which is the basic mode of the turbulence  $\mathbf{k} = (0, 0, 1)$ , whereas during the decreasing

regime, energy is transferred by nonlinearity from the harmonic  $\mathbf{k} = (0, 0, 1)$ . This behavior is attributed to the creation and weakening of a mode with the wavevector  $\mathbf{k} = (0, 0, 1)$  and the Interplay of this process with the processes discussed above will ensure the sustenance of a turbulent state.

So, due to the injection term and the linear drift, perturbations experience transient growth as they are swept through the vital area in  $\mathbf{k}$ -space. Nonlinear transverse cascade redistributes the modes over the wavevector angle, returning part of them in the amplification area. Consequently, turbulence in shear flows is sustained through positive feedback, resulting from the subtle interplay between linear transient growth and the nonlinear transverse cascade processes. Furthermore, the sustenance of turbulence is further influenced by the processes we observed during a small period of time analyzing the generation and decay of bursts.

## 4. Summary and Discussion

In this paper, we investigated the characteristics and self-sustaining mechanism of subcritical 3D turbulence in a spectrally stable MHD shear flow with constant shear and parallel to the flow mean magnetic field by first doing numerical simulations and then analyzing the dynamical processes in Fourier ( $\mathbf{k}$ -)space. We showed that nonlinear processes are anisotropic in  $\mathbf{k}$ -space. This anisotropy arises from the anisotropy of linear processes, which is caused by the shear. Describing this phenomenon within the traditional framework of direct and inverse cascades, commonly used in the classical theory of HD and MHD turbulence without shear, is inadequate, as the primary role of nonlinear processes is to transfer energy across different wavevector orientations (angles) in  $\mathbf{k}$ -space, rather than along the wavevector as in direct/inverse cascades. This new type of nonlinear cascade – the nonlinear transverse cascade – is crucial for providing a positive feedback and thus maintenance of the subcritical turbulence. Indeed, we showed that turbulence is sustained by the subtle interplay of linear nonmodal growth, which injects energy via stresses, and nonlinear transverse cascade, which ensures the regeneration of transiently growing harmonics. This interplay is crucial for self-sustenance of subcritical turbulence. It should be noted that these processes operate at small wave numbers (large length scales) and are referred to as the vital area, where power-consuming processes ensuring the self-sustaining dynamics occur.

We showed that in 3D MHD subcritical turbulence, energy injection into turbulent fluctuations is due to Reynolds stress, in contrast to 2D MHD (Mamatsashvili et al., 2014) and 3D MHD Keplerian flows with different magnetic field configurations (Gogichaishvili et al., 2017, 2018, Mamatsashvili et al., 2020). Therefore, Reynolds stress is responsible for the onset of turbulence in the present case. We also performed numerical simulations for different values of the background magnetic field and demonstrated that as this field increases, the onset of turbulence occurs at larger times and the power of turbulence reduces. Finally, the flow completely stabilizes for  $B_{0y} \approx 0.33$  and higher.

The turbulence exhibits a “bursty” nature, with energy increasing in some time intervals and decreasing in others. Therefore, it becomes important to explore this behavior at small time intervals rather than solely relying on the average effect over the whole saturated state, as the crucial information can be lost. One of the significant findings that we made is that by averaging over small time intervals (in the regions of both energy increase and decrease), we are able to observe dynamics that would otherwise be lost (if considering averaging over whole saturated time). Specifically, we observe the creation and weakening of the dominant large-scale modes  $\mathbf{k} = (0, 0, 1)$ , which plays a key role in the turbulence dynamics and contributes to the self-sustaining process.

### Acknowledgements

M.K. would like to thank supervisor Prof. Nana Shatashvili for all supports, guidance and discussions.

## Appendices

### Appendix A Equations for perturbation components in physical space

Equations governing the evolution of the velocity, total pressure and magnetic field perturbations,  $\mathbf{u}, p, \mathbf{b}$ , about the equilibrium flow  $\mathbf{U}_0 = (0, -Sx, 0)$  with net azimuthal field  $\mathbf{B}_0 = (0, B_{0y}, 0)$  are obtained from the basic Equations (1)-(4) and componentwise have the form:

$$\frac{Du_x}{Dt} = -\frac{1}{\rho_0} \frac{\partial p}{\partial x} + \frac{B_{0y}}{4\pi\rho_0} \frac{\partial b_x}{\partial y} + \frac{\partial}{\partial x} \left( \frac{b_x^2}{4\pi\rho_0} - u_x^2 \right) + \frac{\partial}{\partial y} \left( \frac{b_x b_y}{4\pi\rho_0} - u_x u_y \right) + \frac{\partial}{\partial z} \left( \frac{b_x b_z}{4\pi\rho_0} - u_x u_z \right) + \nu \nabla^2 u_x, \quad (20)$$

$$\frac{Du_y}{Dt} = S u_x - \frac{1}{\rho_0} \frac{\partial p}{\partial y} + \frac{B_{0y}}{4\pi\rho_0} \frac{\partial b_y}{\partial y} + \frac{\partial}{\partial x} \left( \frac{b_x b_y}{4\pi\rho_0} - u_x u_y \right) + \frac{\partial}{\partial y} \left( \frac{b_y^2}{4\pi\rho_0} - u_y^2 \right) + \frac{\partial}{\partial z} \left( \frac{b_y b_z}{4\pi\rho_0} - u_y u_z \right) + \nu \nabla^2 u_y, \quad (21)$$

$$\frac{Du_z}{Dt} = -\frac{1}{\rho_0} \frac{\partial p}{\partial z} + \frac{B_{0y}}{4\pi\rho_0} \frac{\partial b_z}{\partial y} + \frac{\partial}{\partial x} \left( \frac{b_x b_z}{4\pi\rho_0} - u_x u_z \right) + \frac{\partial}{\partial y} \left( \frac{b_y b_z}{4\pi\rho_0} - u_y u_z \right) + \frac{\partial}{\partial z} \left( \frac{b_z^2}{4\pi\rho_0} - u_z^2 \right) + \nu \nabla^2 u_z \quad (22)$$

$$\frac{Db_x}{Dt} = B_{0y} \frac{\partial u_x}{\partial y} + \frac{\partial}{\partial y} (u_x b_y - u_y b_x) - \frac{\partial}{\partial z} (u_z b_x - u_x b_z) + \eta \nabla^2 b_x, \quad (23)$$

$$\frac{Db_y}{Dt} = -S b_x + B_{0y} \frac{\partial u_y}{\partial y} - \frac{\partial}{\partial x} (u_x b_y - u_y b_x) + \frac{\partial}{\partial z} (u_y b_z - u_z b_y) + \eta \nabla^2 b_y, \quad (24)$$

$$\frac{Db_z}{Dt} = B_{0y} \frac{\partial u_z}{\partial y} + \frac{\partial}{\partial x} (u_z b_x - u_x b_z) - \frac{\partial}{\partial y} (u_y b_z - u_z b_y) + \eta \nabla^2 b_z, \quad (25)$$

$$\frac{\partial u_x}{\partial x} + \frac{\partial u_y}{\partial y} + \frac{\partial u_z}{\partial z} = 0, \quad (26)$$

$$\frac{\partial b_x}{\partial x} + \frac{\partial b_y}{\partial y} + \frac{\partial b_z}{\partial z} = 0 \quad (27)$$

where  $D/Dt = \partial/\partial t - Sx\partial/\partial y$  is the total derivative along the background flow.

## References

- Alexakis A., Mininni P. D., Pouquet A., 2007, [New J. Phys.](#), **9**, 298
- Baggett J. S., Driscoll T. A., Trefethen L. N., 1995, [Physics of Fluids](#), **7**, 833
- Chagelishvili G. D., Chanishvili R. G., Lominadze J. G., Tevzadze A. G., 1997, [Phys. Plasmas](#), **4**, 259
- Chagelishvili G., Zahn J.-P., Tevzadze A. G., Lominadze J. G., 2003, [Astronomy & Astrophysics](#), **402**, 401
- Chagelishvili G., Hau J.-N., Khujadze G., Oberlack M., 2016, [Phys. Rev. Fluids](#), **1**, 043603
- Chapman S. J., 2002, [Journal of Fluid Mechanics](#), **451**, 35
- Eckhardt B., Schneider T. M., Hof B., Westerweel J., 2007, [Annual Review of Fluid Mechanics](#), **39**, 447
- Farrell B. F., Ioannou P. J., 1993, [Phys. Fluids](#), **5**, 1390
- Farrell B. F., Ioannou P. J., 1994, [Phys. Rev. Lett.](#), **72**, 1188
- Farrell B. F., Ioannou P. J., 2000, [Phys. Fluids](#), **12**, 3021
- Farrell B. F., Ioannou P., 2012, [Journal of Fluid Mechanics](#), **708**, 149
- Fromang S., Lesur G., 2019, in EAS Publications Series. pp 391–413, [doi:10.1051/eas/1982035](#)
- Gebhardt T., Grossmann S., 1994, [Physical review](#), **50**, 3705
- Gogichaishvili D., Mamatsashvili G., Horton W., Chagelishvili G., Bodo G., 2017, [The Astrophysical Journal](#), **845**, 70
- Gogichaishvili D., Mamatsashvili G., Horton W., Chagelishvili G., 2018, [The Astrophysical Journal](#), **866**, 134
- Grossmann S., 2000, [Reviews of Modern Physics](#), **72**, 603
- Grue J., Kolaas J., Jensen A., 2014, [European Journal of Mechanics - B/Fluids](#), **47**, 97
- Gustavsson L. H., 1991, [Journal of Fluid Mechanics](#), **224**, 241–260
- Henningson D. S., Reddy S. C., 1994, [Physics of Fluids](#), **6**, 1396
- Herault J., Rincon F., Cossu C., Lesur G., Ogilvie G. I., Longaretti P.-Y., 2011, , **84**, 036321
- Horton W., Kim J.-H., Chagelishvili G. D., Bowman J. C., Lominadze J. G., 2010, [Phys. Rev. E](#), **81**, 066304
- Lesur G., Longaretti P.-Y., 2007, [Monthly Notices of the Royal Astronomical Society](#), **378**, 1471
- Lesur G., Ogilvie G. I., 2008, [Astronomy & Astrophysics](#), **488**, 451
- Lominadze D., Chagelishvili G., Chanishvili R., 1988, [Soviet Astronomy Letters](#), **14**, 364
- Longaretti P.-Y., Lesur G., 2010, [Astron. Astrophys.](#) , **516**, A51
- Mamatsashvili G. R., Gogichaishvili D. Z., Chagelishvili G. D., Horton W., 2014, [Phys. Rev. E](#), **89**, 043101
- Kavtaradze et al.  
doi: <https://doi.org/10.52526/25792776-23.70.1-152>

- Mamatsashvili G., Khujadze G., Chagelishvili G., Dong S., Jiménez J., Foysi H., 2016, [Phys. Rev. E](#), 94, 023111
- Mamatsashvili G., Chagelishvili G., Pessah M. E., Stefani F., Bodo G., 2020, [The Astrophysical Journal](#), 904, 47
- Ogilvie G. I., Pringle J. E., 1996, *Mon. Not. R. Astron. Soc.*, **279**, 152
- Reddy S. C., Henningson D. S., 1993, [J. Fluid Mech.](#), **252**, 209
- Reddy S., Schmid P., Henningson D., 1993, *SIAM J. Appl. Math.*, **53**, 15
- Rempel E. L., Lesur G., Proctor M. R. E., 2010, [Phys. Rev. Lett.](#), **105**, 044501
- Schmid P. J., 2007, [Annu. Rev. Fluid Mech.](#), **39**, 129
- Stern M. E., 1963, [Phys. Fluids](#), **6**, 636
- Sundar S., Verma M. K., Alexakis A., Chatterjee A. G., 2017, *Physics of Plasmas*, **24**, 022304
- Teaca B., Verma M. K., Knaepen B., Carati D., 2009, [Phys. Rev. E](#), **79**, 046312
- Tevzadze A. G., Chagelishvili G., Zahn J.-P., Chanishvili R. G., Lominadze J. G., 2003, [Astronomy & Astrophysics](#), **407**, 779
- Trefethen N. L., Embree M., 2005, *Spectra and Pseudospectra: The Behavior of Nonnormal Matrices and Operators*. Princeton University Press, Address
- Trefethen L. N., Trefethen A., Reddy S. C., Driscoll T. A., 1993, [Science](#), **261**, 578
- Verma M. K., 2004, [Physics Reports](#), **401**, 229